Title

Voltage-calibrated, finely tunable protein assembly.

Journal

Journal of the Royal Society Interface, 20(204)

Authors

Lin, Yin-Chen

Masquelier, Eloise

Al Sabeh, Yahya

et al.

Publication Date

2023-07-01

DOI

10.1098/rsif.2023.0183

Peer reviewed

INTERFACE

royalsocietypublishing.org/journal/rsif

Research

Cite this article: Lin Y-C, Masquelier E, Sabeh YA, Sepunaru L, Gordon MJ, Morse DE. 2023 Voltage-calibrated, finely tunable protein assembly. *J. R. Soc. Interface* **20**: 20230183. https://doi.org/10.1098/rsif.2023.0183

Received: 28 March 2023
Accepted: 12 June 2023

Subject Category:
Life Sciences–Chemistry interface

Subject Areas:
biomaterials, biophysics, biotechnology

Keywords:
reflectin, electrochemistry, spectroscopy, protein assembly

Author for correspondence:
Daniel E. Morse
e-mail: d_morse@lifesci.ucsb.edu

†To whom inquiries should be addressed.

Electronic supplementary material is available online at https://doi.org/10.6084/m9.figshare.c.6707535.

THE ROYAL SOCIETY PUBLISHING

Voltage-calibrated, finely tunable protein assembly

Yin-Chen Lin[1,2], Eloise Masquelier[1,3], Yahya Al Sabeh[1,4], Lior Sepunaru[5], Michael J. Gordon[1,2] and Daniel E. Morse[1,4,†]

[1]Institute for Collaborative Biotechnologies, [2]Department of Chemical Engineering, [3]Materials Department, [4]Department of Molecular, Cellular and Developmental Biology, and [5]Department of Chemistry and Biochemistry, University of California, Santa Barbara, CA 93106, USA

Y-CL, 0009-0006-0614-3426; EM, 0000-0003-1380-3104; LS, 0000-0002-4716-5035; MJG, 0000-0003-0123-9649

Neuronally triggered phosphorylation drives the calibrated and cyclable assembly of the reflectin signal transducing proteins, resulting in their fine tuning of colours reflected from specialized skin cells in squid for camouflage and communication. In close parallel to this physiological behaviour, we demonstrate for the first time that electrochemical reduction of reflectin A1, used as a surrogate for charge neutralization by phosphorylation, triggers voltage-calibrated, proportional and cyclable control of the size of the protein's assembly. Electrochemically triggered condensation, folding and assembly were simultaneously analysed using *in situ* dynamic light scattering, circular dichroism and UV absorbance spectroscopies. The correlation of assembly size with applied potential is probably linked to reflectin's mechanism of dynamic arrest, which is controlled by the extent of neuronally triggered charge neutralization and the corresponding fine tuning of colour in the biological system. This work opens a new perspective on electrically controlling and simultaneously observing reflectin assembly and, more broadly, provides access to manipulate, observe and electrokinetically control the formation of intermediates and conformational dynamics of macromolecular systems.

1. Introduction

Cephalopods are well known for their remarkable capabilities to manipulate light for camouflage and communication [1–4]. Of these systems, the dynamically tunable colour and intensity of iridescence reflected from skin cells in certain squids have emerged as an inspiration for next-generation applications in advanced optical materials and devices [5–8]. The mechanisms that squids employ to modulate changes in reflected light are regulated by the reflectin proteins, the major constituents in the stacks of plasma membrane-bounded lamellae (iridosomes) within the specialized 'iridocyte' skin cells [5,9–12]. This cellular 'superstructure' functions as a tunable Bragg reflector consisting of alternating layers of high refractive index platelets and low refractive index extracellular space [13–16]. Reflectin A1, the majority species, is a block copolymer-like peptide chain of *ca* 350 amino acid residues consisting of six repeating conserved domains alternating with cationic linkers, of which the positive charge is dominated by a total of 31 histidines [13,17]. *In vivo*, progressive charge neutralization by neurotransmitter-activated phosphorylation overcomes the Coulombic repulsion of reflectin's cationic linkers to drive condensation, folding and assembly [18,19]. Assembly then triggers osmotic and Gibbs–Donnan-mediated dehydration of the Bragg lamellae, reducing the platelet thickness and spacing, while increasing refractive index, thus dynamically tuning the colour of the reflected light [20–22]. *In vitro*, pH-titration, charge screening and genetic engineering function as surrogates for *in vivo* phosphorylation, progressively neutralizing the initially cationic reflectin to monotonically drive assembly calibrated with the extent of charge neutralization [19,23,24].

Recently, study has shown that dissociable protons of free and peptide-incorporated amino acids can be directly electroreduced at a bare platinum electrode with reduction potentials correlated with their pKa values [25]. Liang *et al*. demonstrated that low-voltage electrochemical reduction can selectively target the deprotonation of histidine residues in histidine-rich reflectin A1, driving and simultaneously measuring its assembly [17]. In those experiments and the ones we present here, acidic conditions were used to ensure the protein's initial full protonation, thus starting each experiment from its unstructured monomeric state. Combining electrochemistry with dynamic light scattering (E-DLS), these observations first showed that electrochemistry can provide a simple and convenient approach to probe a protein's thermodynamics while controlling its charge and assembly. However, the effects of voltage level in the evolution of reflectin assembly and the accompanying changes in its secondary structure remained unknown. Masquelier *et al*. showed that combining electrochemistry with *in situ* circular dichroism and UV absorbance spectroscopies (E-CD) can be used to simultaneously trigger and analyse the evolution of secondary structure in polylysine [26]. Inspired by these findings, we used E-DLS and E-CD to trigger and quantitatively analyse conformational transitions of reflectin A1 as a function of electrochemical potential applied to the Pt electrode in real time. The catalytic efficiency of the Pt working electrode, for which the physical mechanism of proton electroreduction has been recently clarified [27], allows the dual advantages of low-voltage electroreduction of histidine residues in proteins, and reduction at potentials that are distinct from those driving both hydronium reduction and water hydrolysis. The results demonstrate for the first time that reflectin assembly size can be proportionally tuned by applied potential, as previously observed for the protein's response to neuronally triggered phosphorylation *in vivo* and to charge neutralization by pH titration, charge screening and genetic engineering *in vitro* [19,23]. The well-defined size observed at each voltage suggests that assembly is limited by a dynamic equilibrium at the electrode's diffusion layer, thus exhibiting the same mechanism that is responsible for the precise calibration between the neuronally triggered charge neutralization and colour in the squid [23]. Also significantly, our analyses demonstrate rapid and complete reversibility of reflectin assembly when the applied potential is turned off, and repeated cyclability of assembly and disassembly in response to voltage being turned on and off, in this first example of a protein's cyclable assembly controlled electrochemically as it is biochemically.

2. Results and discussion

2.1. Differential pulse voltammetry of reflectin

To identify the electrochemical reduction potential of histidines inside reflectin, differential pulse voltammetry (DPV) was performed on 25 µM reflectin in 40 mM NaCl (to ensure conductivity) at pH 3. This electrolyte condition was chosen to guarantee full protonation of all the protein's constituent amino acids, sufficient ionic conductivity and a low background of UV absorption in the wavelength region probed. The DPV of reflectin (figure 1*a*) exhibits a distinct electroreduction wave at −0.45 V with a shoulder around −0.57 V (black, solid curve). In comparison with the blank solution (black, dashed curve), the reduction peak at −0.45 V is the signature of hydronium reduction in the acidic, aqueous solvent [17,26,27]. The shoulder at −0.57 V, which becomes increasingly evident after deconvolution (orange curve), corresponds to reduction of the imidazolium side-chain of histidine residues in the protein [17,25].

2.2. Electrochemical dynamic light scattering of reflectin assembly

Potentials below and above reflectin's identified reduction peak at −0.57 V versus Ag/AgCl were selected to analyse the time-dependent evolution of reflectin assembly size during electrochemical activation by E-DLS, allowing us to simultaneously drive and quantitatively monitor these processes (figure 1*b–f*) using the experimental set-up shown in the electronic supplementary material, figure S1. The subthreshold potential of −0.475 V, sufficient to reduce hydronium ion, produces no change in reflectin size over that of the *ca* 10 nm monomer (figure 1*b*). This result indicates that the electrochemically driven pH gradient resulting from hydronium reduction near the working electrode is insufficient to trigger reflectin assembly. By contrast, the slight increase in applied voltage to −0.57 V triggers metastable assembly over 25 min, with rapid return to the starting size of the monomer when the potential is returned to open circuit potential (OCP) (i.e. equilibrium potential at which no current is flowing in the cell) (figure 1*c*). The observed metastability of assembly can be attributed, in this kinetically controlled regime, to the rate of assembly being just barely able to compete with disassembly caused by the surrounding low-pH environment. At the higher potential of −0.6 V, reflectin assembly size is stable and homogeneous. Again, disassembly to monomers quickly occurs when the applied voltage is turned off, indicating rapid and complete reversibility. Similarly, progressively larger assemblies are observed at −0.7 and −0.8 V, with rapid disassembly to the monomers driven by diffusion into the low pH environment and the return to local acidic environment at the electrode surface, once the voltage is turned off (figure 1*e*,*f*). In addition, the pH gradient that arises from a small level of water electrolysis at a potential of −0.8 V may also contribute to reflectin assembly. As such, potentials below −0.8 V that can generate larger pH gradients have not been discussed here.

Under apparent steady-state conditions (after 25 min), the final sizes of reflectin assemblies are seen to have increased monotonically as a function of negative potential applied to the working electrode (figure 2*a*). (A control DLS analysis in the absence of added salt is shown for comparison in the electronic supplementary material, figure S2). After a threshold, the results are in close parallel to the protein's assembly in proportional response to the neuronal signal and its charge-neutralizing phosphorylation *in vivo*, and to charge neutralization by pH titration, charge screening and genetic engineering *in vitro* [11,23]. At −0.8 V, reflectin exhibits the largest assembly size (60 ± 20 nm), compared with the results at −0.7 V (50 ± 20 nm), −0.6 V (35 ± 15 nm), −0.57 V (27 ± 13 nm) and −0.475 V (10 nm = approximate diameter of the monomers). Although the size distribution *by volume* at −0.8 V displays a mixture of two reflectin assembly sizes, only the smaller of these is shown in figure 2*b*, since it accounts for 99.6% of the *particle number*. Data are consistent with the hypothesis that at progressively higher voltages,

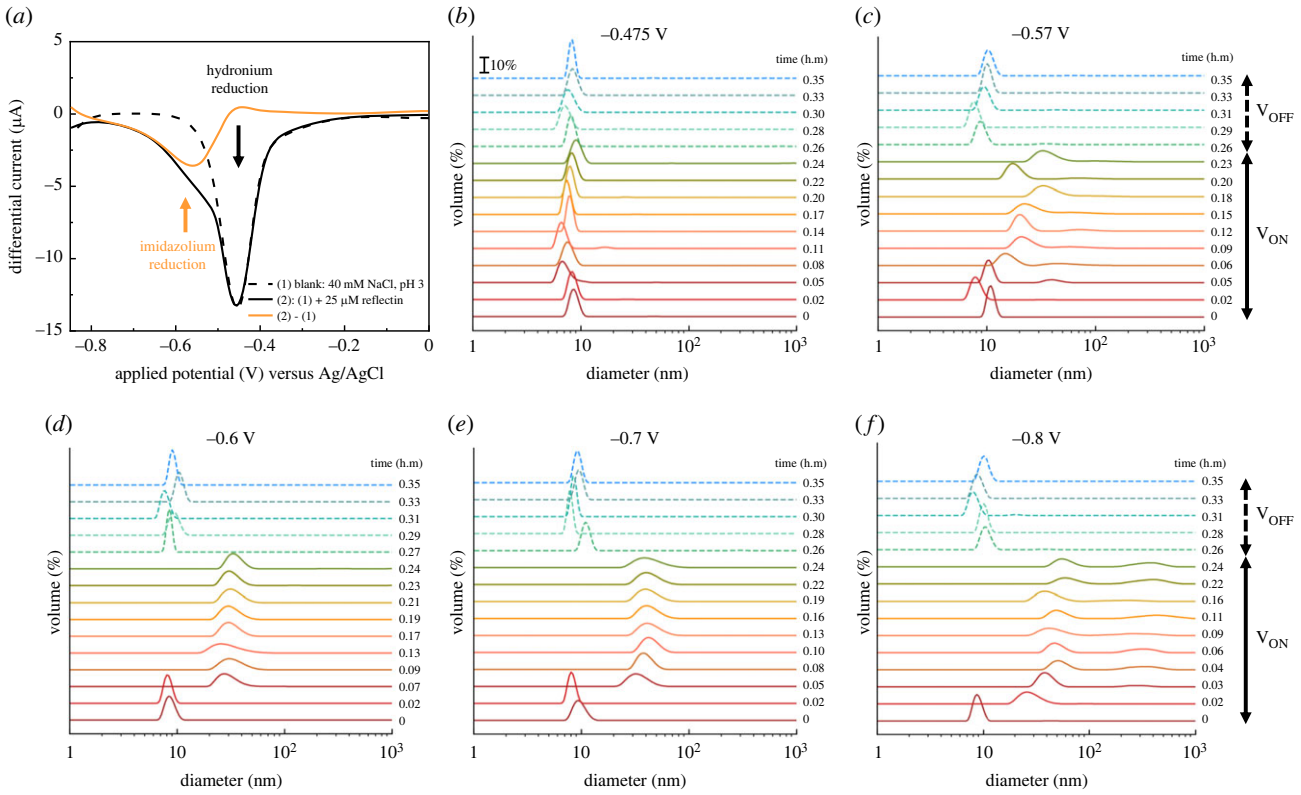

Figure 1. Electroreduction of histidine imidazolium in reflectin and evolution of assembly size as a function of voltage during electrochemical activation. (*a*) DPV of 25 µM reflectin in 40 mM NaCl, 1 mM perchloric acid, pH 3. Orange curve is the deconvolved voltammogram of reflectin after subtraction of the DPV without reflectin (dashed line) from the DPV with reflectin (black). (*b–f*) *In situ* dynamic light scattering (E-DLS) of particle size distribution of 2 µM reflectin in 40 mM NaCl, 1 mM perchloric acid, pH 3 at applied voltages of (*b*) −0.475 V, (*c*) −0.57 V, (*d*) −0.6 V, (*e*) −0.7 V and (*f*) −0.8 V. DLS was continuously measured during application (V_{ON}) and after the potential was returned to open circuit potential (OCP) (V_{OFF}) (solid and dashed lines, respectively).

histidine residues with slightly greater than their prototypical pKa, possibly due to differences in local sequence environment or steric hindrance, are electroreduced to yield progressively larger assemblies [25]. These histidine residues with various pKa may be observed and evidenced by the relatively broad reduction peak of reflectin (figure 1*a*).

Interestingly, the threshold for assembly seen in figure 2*b*, *c* indicates a small barrier, suggesting that electroreduction of a sufficient number of histidine residues is required for assembly. This suggestion is experimentally confirmed by the inability of −0.55 V, a voltage capable of reducing the imidazolium of free histidine [25], to trigger assembly of reflectin A1 (electronic supplementary material, figure S3). This barrier was similarly observed in the protein's pH-dependent assembly with values lower than the pKa of histidine being ineffective [23].

The relation between the rate of reflectin assembly and voltage was further investigated by analysing assembly size over the first 10 min after application of −0.6, −0.7 and −0.8 V (figure 2*c*; electronic supplementary material, figure S4). The results unequivocally reveal that more negative potentials rapidly drive assemblies to the same sizes, owing to both the electroreduction of more histidines and the potentially faster electron transfer rate indicated by the broad and asymmetric reduction peak in reflectin's DPV (figure 2*b*). For example, the formation of assemblies of *ca* 30 nm diameter requires approximately 2 and 6 min with applied potentials of −0.6 and −0.8 V, respectively. Thus, both the rate and size of reflectin assembly increase monotonically as a function of electrical signal strength. The observed lag time before the onset of any detectable increase in diameter (figure 2*c*) is progressively decreased with more negative potentials (figure 2*d*), consistent with our hypothesis that more rapid assembly occurs under more negative potentials. (Although the lag times observed for the two lowest voltages are the same, this is a consequence of the relatively low temporal resolution of analysis, as indicated by the larger assembly size at −0.6 V relative to that at −0.57 V.)

To gain further insight into the assembly process triggered by electrochemistry, the count rates of back-scattered photons from the DLS photodetector at different potentials were measured simultaneously with the determination of size, since the intensity of Rayleigh scattering depends on both the sixth power of the diameter and the absolute number of light-scattering particles [17]. Initially, similar count rates were observed at each voltage analysed, since each sample contained the same concentration and number of reflectin monomers (figure 3*a*). The insufficient driving force of −0.475 V did not increase count rate as a function of time (figure 3*a*), consistent with the lack of assembly already noted (figures 1 and 2). By contrast, count rate began to climb at increasingly faster rates and reach correspondingly higher plateaus, monotonically as a function of progressively greater negative potentials (figure 3*a*), consistent with the assembly sizes described above (figures 1 and 2). The stable plateau values are parallel to the results previously observed using pH titration as a surrogate for charge neutralization resulting from phosphorylation *in vivo*, in which the assemblies remained stable with both time and dilution. Significantly, the count rate in all samples falls precipitously as soon as the applied voltage is turned off, consistent with the disassembly to monomers as described above.

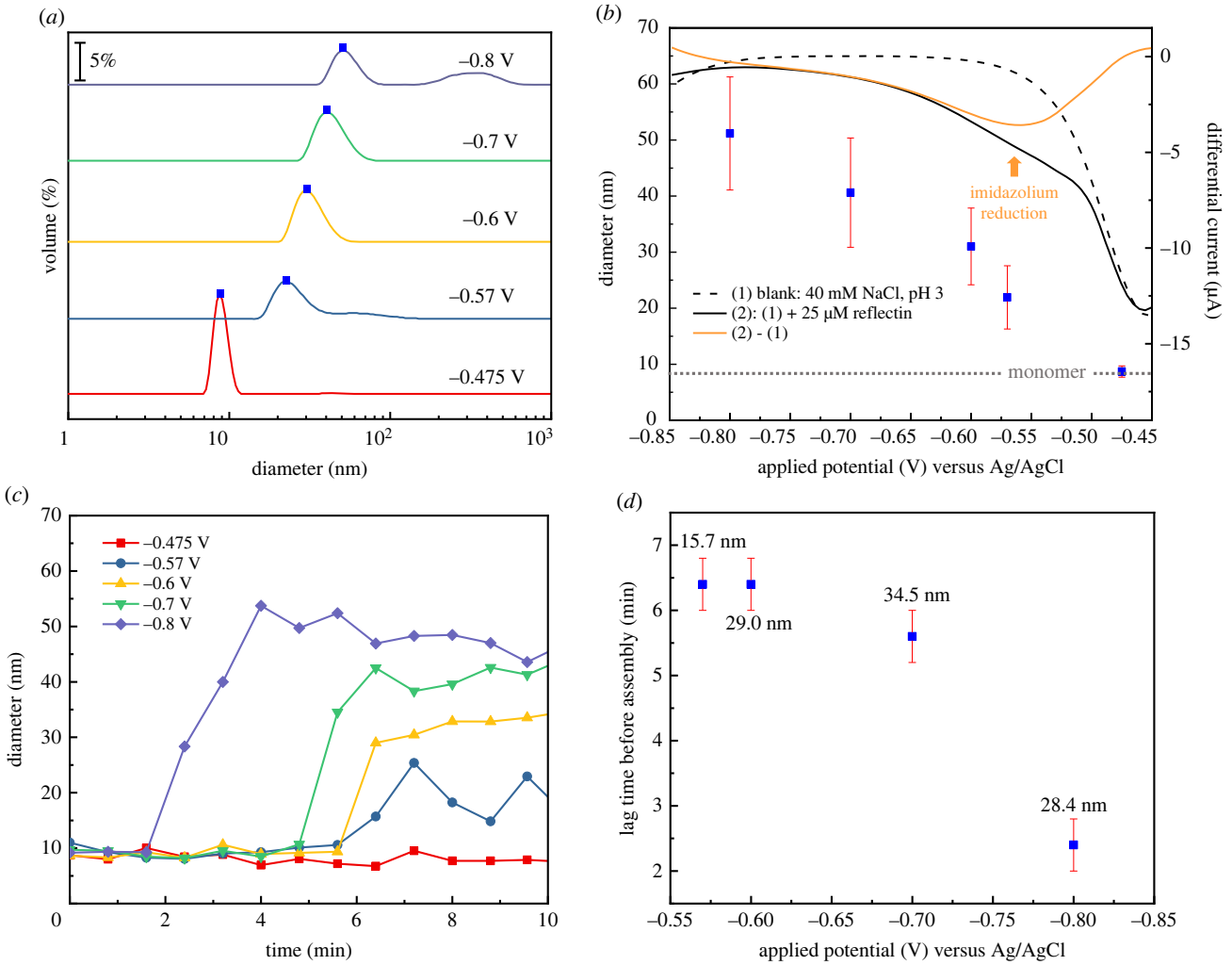

Figure 2. Reflectin assembly rate and size as a function of voltage. (*a*) Final reflectin size distributions and (*b*) assembly sizes (left axis) measured by DLS with specified voltage applied for 25 min; error bars indicate full width at half maximum. DPV (right axis) was included for reference. (*c*) Evolution of assembly size as a function of applied voltage over the first 10 min. (*d*) Lag time between application of the specified potential and first observed increase in assembly size (i.e. larger than monomer, approx. 10 nm) in *c*. Vertical error bars correspond to the time between sampling points. All solutions were 2 μM reflectin in 40 mM NaCl, 1 mM perchloric acid, pH 3.

These results are consistent with the evolution of particle size distributions in figure 1*b–f*. Figure 3*b* reveals the lag time at different potentials before any onset of increase in the count rate as seen in figure 3*a*. The more negative voltages exhibit progressively shorter delay, indicating that less time is required for sufficient charge neutralization to trigger assembly. This 'lag' in count rate increase (figure 3*b*) falls more rapidly as a function of voltage than the corresponding lag in growth of assembly size (figure 2*d*), simply because the count rate of photon scattering is a function of both particle number and particle diameter. The latter power law dependency greatly magnifies the contribution of relatively small increases in particle diameter (shown above each voltage in figure 2*d*). The slope of count rate also increases monotonically with increasingly negative applied voltage (figure 3*c*), consistent with voltage-dependent increases in both assembly particle number and size (cf. Figure 2*d*).

To further investigate the phenomenon of dynamic arrest, E-DLS was performed on reflectin A1 at three different concentrations (1, 2 and 3 μM) with an applied potential of –0.7 V (electronic supplementary material, figure S5). All measurements were conducted in 40 mM NaCl to ensure consistency. Interestingly, we observe that the final assembly size does not depend on the initial monomer concentration (electronic supplementary material, figure S5). The presence of similar sizes confirms the precise and finely tunable relationship between the extent of charge neutralization and the resulting size of reflectin assemblies that *in vivo* ensures the accurate calibration between the triggering neurochemical signal and the resulting changes in skin colour of squid [23]. Since the assembly sizes are comparable at these three concentrations, the increases in the plateaus of count rate (electronic supplementary material, figure S6*a*,*b*) primarily depend on the *number* of assembled particles in the system. In contrast, little if any difference in the count rate slope is observed as a function of reflectin concentration, consistent with the unchanged rate of electron transfer and thus unchanged kinetics of assembly at the electrode (electronic supplementary material, figure S6*c*).

2.3. Electrochemical circular dichroism of conformational transition

To evaluate the conformational response of reflectin to heterogeneous charge neutralization resulting from the electroreduction of histidine residues, *in situ* circular dichroism (E-CD) and UV absorbance were measured during electrochemistry (figure 4). The ellipticity of reflectin shows strong minima

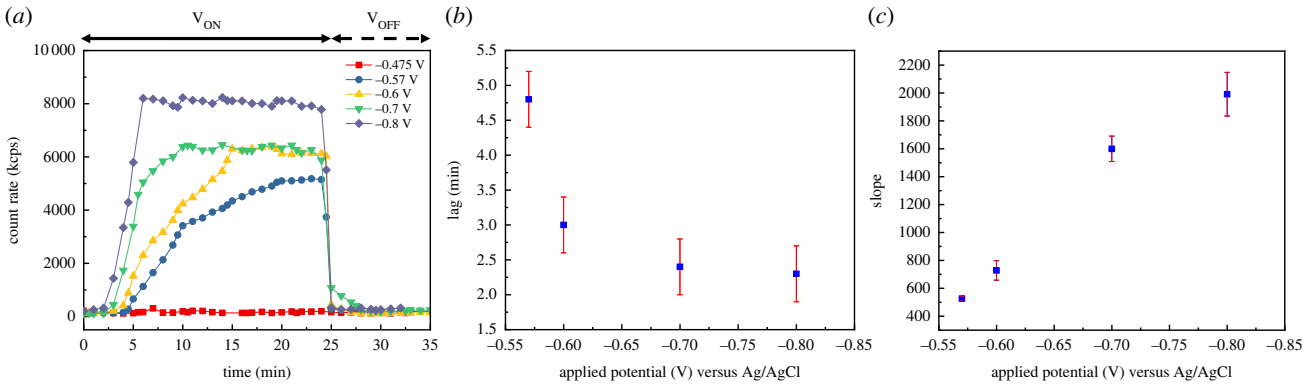

Figure 3. Plateaus of count rate show dynamic arrest of reflectin assembly. (*a*) Count rates from the DLS photodetector, continuously measured during and after application of the specified voltage. (*b*) Lag time between application of specified potential and increase of the count rate. Error bars correspond to the measurement time. (*c*) Slope of the count rate versus time from panel *a* in units of (kcps min^{-1}) for different applied potentials, calculated from a linear fit of the initial rise in count rate. Error bars show ± s.d. All solutions were 2 µM reflectin in 40 mM NaCl, 1 mM perchloric acid, pH 3.

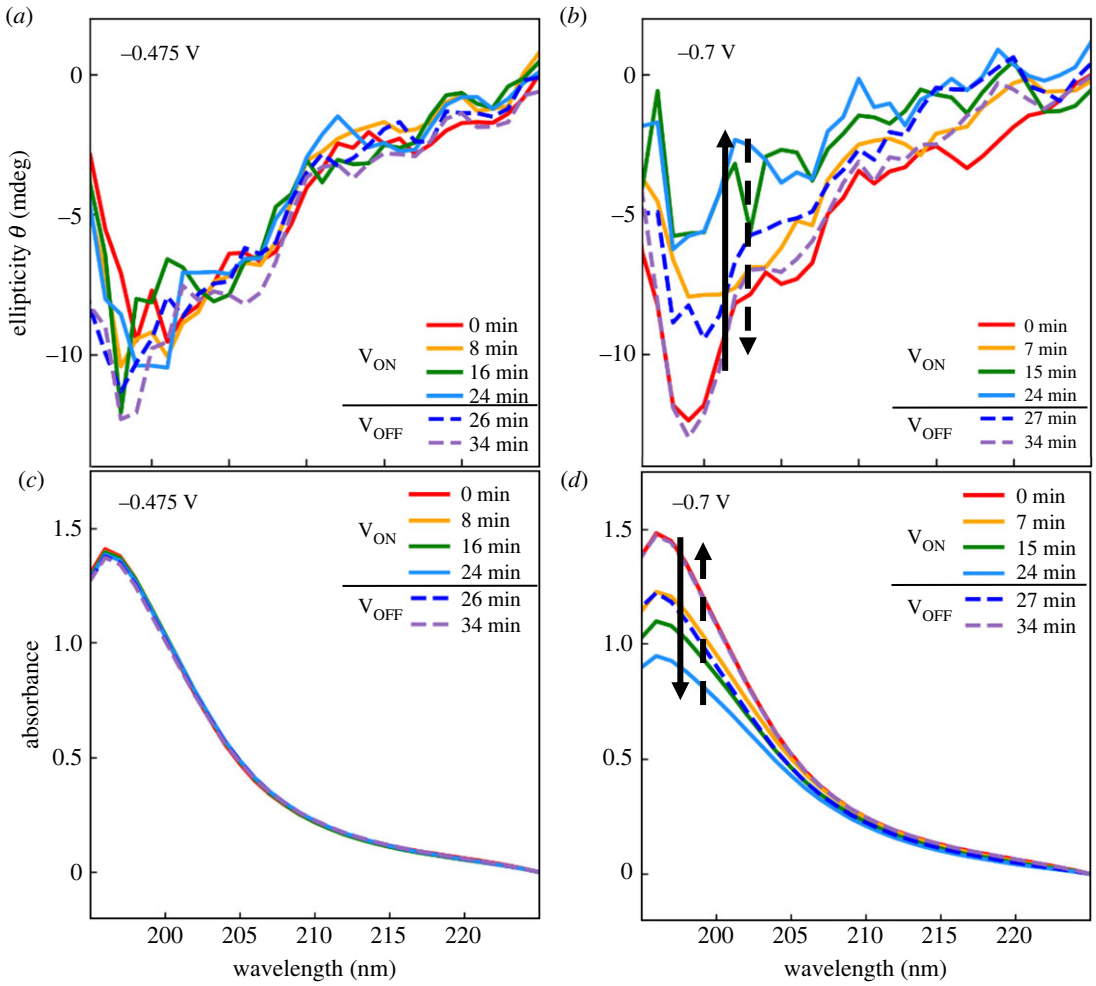

Figure 4. Electroreduction of reflectin drives secondary folding. Dynamic evolution of ellipticity (*a*,*b*) and absorbance (*c*,*d*) of 2 µM reflectin in 40 mM NaCl, 1 mM perchloric acid, pH 3 exposed to an applied potential of (*a*,*c*) −0.475 V and (*b*,*d*) −0.7 V. CD was continuously monitored during this exposure (V_{ON}) and after the potential was returned to OCP (V_{OFF}) (solid and dashed curves, respectively). Solid and dashed arrows indicate the temporal evolution of CD and absorbance signals during and following exposure to potential, respectively.

near 200 nm at 0 min, corresponding to a random coil conformation of protein [28]. Control CD analyses in the absence of added protein or salt are shown in the electronic supplementary material, figure S7 for comparison. At a low potential of −0.475 V, the ellipticity and absorbance remain stable over time (figure 4*a*,*c*), demonstrating no structural change at a potential that produced no assembly (figures 1–3). In marked contrast at −0.7 V, ellipticity gradually evolves near 200 nm (figure 4*b*; electronic supplementary material, figure S8), suggesting significant structural changes during assembly. Previous analyses showed that the CD spectrum of reflectin assemblies is consistent with the presence of both α-helix and β-sheet structures [23,28]. The unresolved spectra of these structures at 208–220 nm may partially be due to the inhomogeneous nature of the sample, consisting of assemblies near the electrode and monomers in the surrounding acidic medium.

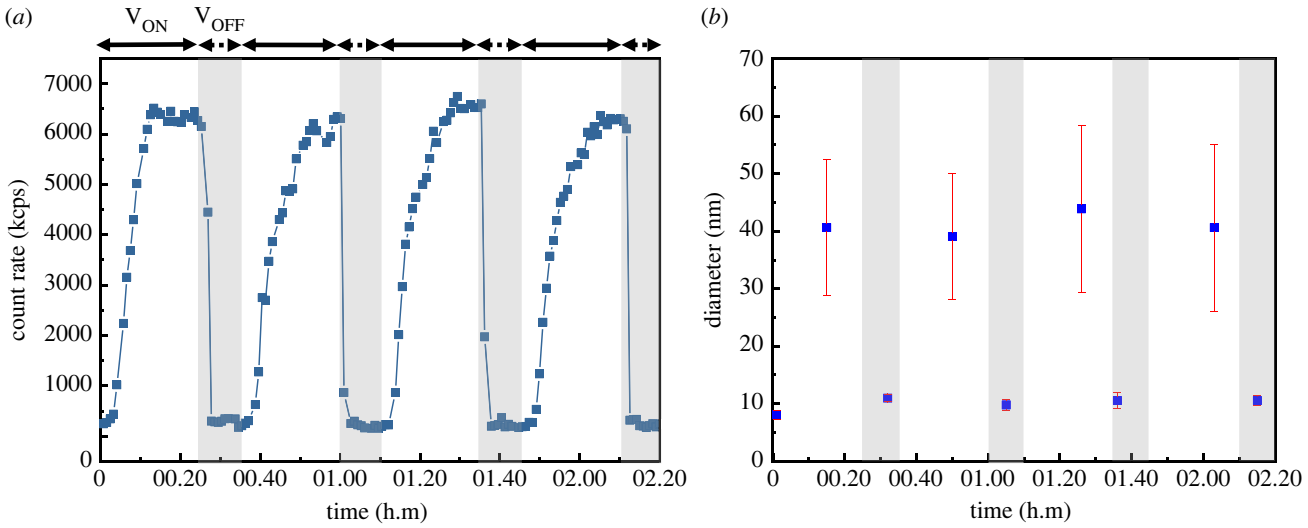

Figure 5. Reversibility and cyclability of reflectin's electro-assembly. (*a*) Count rate of reflectin assembly and disassembly measured by E-DLS as a function of time during four cycles of 25 min exposure to −0.7 V (V_{ON}) followed by 10 min at OCP (V_{OFF}). (*b*) Corresponding sizes at stages indicated in (*a*). Error bars show the full width at half maximum of reflectin particle size distribution. Reflectin (2 µM) in 40 mM NaCl, pH 3.

Voltage- and time-dependent changes in UV absorbance (figure 4*d*) parallel those in CD and assembly, with significant hypochromicity at *ca* 197 nm, corresponding to the induced conformational transition from a random coil to α-helix [29,30]. This transition is attributed to the strong dipole–dipole interactions between the chromophoric peptide bonds as they take up the α-helical conformation [31,32]. Notably, as soon as the potential is switched off, the protein reverts back to the random coil conformation in response to the low pH environment (figure 4*b*,*d*). This result is in good agreement with the aforementioned disassembly as seen by E-DLS size distribution and count rate (figures 1–3).

2.4. Reversibility and cyclability

In efforts to mimic the reversibility and cyclability of reflectin folding and assembly occurring in the tunable squid iridocytes, E-DLS was conducted with potential switched on and off for several cycles (figure 5). Figure 5*a* shows the similar rise and fall of count rate in each of four cycles, and the corresponding sizes at indicated times are displayed in figure 5*b* and electronic supplementary material, figure S9. These results indicate that reflectin A1 reversibly switched through multiple cycles of assembly and complete disassembly. This is the first time that such electrically driven, reversible assembly has been demonstrated for any protein. While this switching behaviour of reflectin also can be driven by cyclical changes in pH [19], the need for dialysis (to prevent increases in salt concentration) make that process slow, while the electrochemical process shown here is quicker and potentially more practical for future applications such as photochemical switching.

3. Conclusion

The results reported here build on the prior demonstration that charge neutralization by low-voltage electroreduction can serve as a surrogate for signal-dependent phosphorylation to trigger protein folding and assembly [17,33]. What is new here is the demonstration that protein assembly, which can be proportionally driven by phosphorylation *in vivo*, can be size-proportionally driven by small increments of DC voltage *in vitro*. The rate of assembly (as inferred from the DLS count rate, which convolves both number density and size) also appears to increase with voltage. The physical mechanism and utility of this process differs completely from those of AC field-mediated concentration, liquid–liquid phase segregation and crystallization of macromolecules [34–37].

The data presented demonstrate for the first time that low-voltage electrochemical reduction monotonically, reversibly and cyclically fine-tunes the rate and size of reflectin A1 assembly as a function of voltage in acidic media. Assembly is triggered, at least in part, by what appears to be direct deprotonation of the imidazolium side-chains of histidine residues in reflectin at a Pt surface at a potential above reflectin's identified reduction peak of −0.57 V. Inspection of the DPV data (figure 1*a*), however, reveals that a pH gradient will exist at these potentials, extending from alkalinity in the vicinity of the working electrode to the acidity of the bulk solution, thus raising the possibility that some charge neutralization may result from electrochemically driven pH titration. Related spectro-electrochemical analyses of charge neutralization-driven conformational transition of polylysine confirm that direct electroreduction of protein does occur at the electrode surface under these conditions [26]. Our current investigations are seeking to define the relative contributions of these two processes and the factors that control them.

E-DLS was used to simultaneously trigger and dynamically monitor the evolution of reflectin assembly size from the *ca* 10 nm diameter monomers (at zero applied voltage) to 15–40 nm diameter assemblies at −0.57 V; 20–50 nm at −0.6 V; 30–70 nm at −0.7 V and 40–80 nm at −0.8 V. The precise relationship between voltage and the resulting size is governed by the protein's rapid dynamic equilibration of assembly size as a function of its net charge [23]. This behaviour, responsible for reflectin's precise calibration between neuronally driven, phosphorylation-mediated charge neutralization and colour in the biological (squid skin cell) system, is likely to result from the balance between the protein's weak, short-range attractive forces and its stronger, long-range repulsive (primarily Coulombic) forces, as characteristic of

many colloidal systems [38,39] and consistent with the observed tuning with charge [23] and voltage. The rate of assembly also increases monotonically with applied voltage, permitting very fine tuning.

The mechanism by which charge neutralization reversibly and cyclically controls reflectin's structure and assembly is fairly well understood [16,19,23]. Reflectin A1 is a cationic, alternating block copolymer-like protein, with six histidine-rich cationic linkers separating six unique conserved domains, and functions like a concatanate of alternating opposing mechanical springs [19]: analyses showed that Coulombic repulsion of the cationic domains opposes the thermodynamic drive of the conserved domains to condense and fold [16,19,23]. Progressive charge neutralization, by phosphorylation *in vivo*, or by genetic engineering, pH-titration (or electroreduction) *in vitro*, progressively overcomes that Coulombic repulsion, allowing condensations and folding of the conserved domains to alpha and beta structures creating newly emergent hydrophobic surfaces suggested to facilitate hierarchical assembly [16,17,19,23]. Sites of phosphorylation are located in several of the cationic linkers [13], consistent with the results of deletion analyses and titration analyses [19] confirming that the 'Coulombic switch' governing assembly is spatially disseminated along the protein chain. Previous genetic deletion experiments showed that the reduction of any specific histidine is not required to trigger folding and assembly; instead, it is simply the net charge balance of the protein that matters [19].

The systematic variation in lag time with voltage before the onset of increase in count rate (measured by E-DLS) indicates that the applied potential is critical to determining the time required to achieve sufficient charge neutralization for assembly. E-CD and UV absorbance were analysed to evaluate the conformational response of reflectin to charge neutralization resulting from electroreduction. The results confirmed the electrochemically driven evolution from the initial random coil conformation of the fully protonated reflectin monomer (with Coulombic repulsion of the cationic linkers preventing both folding and assembly [9,23]) to α-helix and β-structures concomitant with assembly.

Previous analysis of the interacting effects of salt concentration and pH on reflectin's structure and assembly showed that the principal effect of salt is through charge screening [39]. This contributes an independent axis of charge neutralization that can be manipulated to increase or decrease a protein's sensitivity to electrochemically driven folding and assembly, thus potentially increasing the power of the methods described here.

In summary, our findings demonstrate that electrochemistry can be used as a surrogate for stimulus-regulated phosphorylation, precisely regulating protein charge state to enable the simultaneous fine tuning and analysis of protein folding and assembly. The significance, wide generality and potential utility of this finding extends far beyond the squid's signal transducing reflectin, as signal-controlled phosphorylation is one of the most evolutionarily ancient and widely distributed mechanisms regulating protein structure and function throughout the kingdom of life. As one further example, we note that low-voltage electroreduction drives assembly of K18, the core peptide of tau—the brain protein that is pathologically driven by excess phosphorylation to assemble as amyloid in Alzheimer's and related neurodegenerative diseases [33]. The structural features shared by reflectin and K18 that enable their responses to be tuned by electroreduction include their thermodynamic drive to fold and assemble [16]; the restriction of that drive by the Coulombic repulsion of their cationic residues (primarily histidine in the case of reflectin, and lysine in the case of K18) initially maintaining both as intrinsically disordered proteins, and their physiological regulation by signal-activated phosphorylation, progressively neutralizing Coulombic repulsion to drive proportional folding and assembly. For both reflectin and K18, low-voltage electroreduction (of His^+ or Lys^+, respectively) acts as a surrogate for charge-neutralizing phosphorylation to permit the proteins' entropically driven [16] folding and assembly. Our results with reflectin (from squid) and K18 (from human brain) suggest that this regulatory mechanism, in which cationic, Coulombic repulsion inhibits the drive for protein folding and assembly, and signal-dependent phosphorylation progressively overcomes that inhibition in a quantized manner, may in fact be widely distributed in biological systems. In the case of reflectin A1, the rates and sizes of assembly are closely and monotonically calibrated with voltage, and reversible and repeatedly cyclable, all in close parallel with these behaviours finely tuned by charge neutralization physiologically by phosphorylation, and *in vitro* by pH titration, charge screening and genetic engineering [23]. These results open new avenues for manipulating other macromolecular systems, designing advanced functional materials and devices, and bridging the biotic–abiotic interface.

4. Methods

4.1. Reflectin source, expression and purification

Recombinant reflectin A1 from the squid, *Doryteuthis opalescens*, was produced from a codon-optimized DNA construct, expressed in Rosetta 2 (DE3) *E. coli*. It was then purified by centrifugal collection of the protein expressed as inclusion bodies, followed by chaotropic solubilization, cation exchange and reverse-phase chromatographies, all as previously described [19]. The purified protein was lyophilized and stored at −80°C until solubilized for use [23]. Purity and functional integrity were confirmed by SDS-PAGE and assembly as a function of pH as measured by DLS, also as previously [23].

4.2. Reflectin solubilization and sample preparation

Lyophilized reflectin was dissolved in 0.22 µm-filtered sodium acetate buffer (25 mM, pH 4.5), and concentration determined by spectroscopic measurement of A_{280} [23]. For electrochemical measurements, solubilized reflectin was then diluted into 40 mM NaCl, 1 mM $HClO_4$, pH 3 to final protein concentrations of 1, 2, 3 and 25 µM. Final pH values were readjusted to 3.0 by the addition of $HClO_4$ as needed.

4.3. Differential pulse voltammetry measurements

Reflectin DPV was conducted in 20 µl droplets of analyte (25 µM reflectin in 40 mM NaCl, 1 mM $HClO_4$, pH 3) using an Autolab M204 electrochemical workstation with a standard three-electrode configuration consisting of a 2 mm diameter Pt disc as working electrode, a Pt wire as counter electrode, and a fritted Ag/AgCl in 1 M KCl aqueous solution as reference electrode. The analyte solution was centred on the working electrode faced upward with the reference electrode on top and the counter electrode inserted between the working and reference electrode. Before each measurement, the Pt disc working electrode was

polished successively with 3, 1, 0.25 and 0.05 µm MetaDiTM polycrystalline diamond suspensions (Buehler, Lake Bluff, IL, USA) on a micro-fibre cloth polishing pad, after which the polished working electrode was sonicated in water for 2 min. DPV measurements were performed with a potential step size of 5 mV, pulse height of 10 mV, pulse duration of 50 ms and interval time of 0.5 s [40].

4.4. Electrochemically driven *in situ* dynamic light scattering

In situ DLS measurements of reflectin (2 µM in 40 mM NaCl, 1 mM $HClO_4$, pH 3) were conducted using Autolab M204 electrochemical workstation used in chronoamperometry mode with a three-electrode configuration consisting of a Pt coil as working electrode, a Pt wire as counter electrode and a fritted Ag/AgCl in 1 M KCl aqueous solution as reference electrode assembled in a DLS compatible optical cuvette and sealed with a plug to avoid evaporation and dust. DLS was carried out with a Malvern Zetasizer Nano ZS, aways at the same scanning frequency, as previously described and illustrated [17]. All samples were measured with a 632.8 nm HeNe gas laser with a beam diameter of 0.63 mm ($1/e^2$) and detected by an avalanche photodiode (quantum efficiency (QE) greater than 50% at 633 nm) in a back-scattering configuration at 7° from normal. Measurements were performed with 1.2 ml sample volumes at 25°C at the potentials indicated for 25 min and then followed with bias off for 10 min. Cyclability of reflectin was evaluated at −0.7 V for 25 min and followed with bias off for 10 min for four cycles.

4.5. Electrochemically driven *in situ* circular dichroism

In situ CD measurements of reflectin (2 µM in 40 mM NaCl, 1 mM $HClO_4$, pH 3) were performed on a Jasco J-1500 spectropolarimeter with constant N_2 flushing, temperature controlled at 25°C and a Gamry electrochemical workstation used in chronoamperometry mode with a three-electrode configuration consisting of a Pt mesh (52 mesh Pt wire of 100 µm diameter folded in two, geometric area = 8 × 16 mm^2) as working electrode, a Pt mesh (52 mesh Pt wire of a 100 µm diameter folded in two, geometric area = 4 × 8 mm^2) as counter electrode, and a fritted Ag/AgCl in 1 M KCl aqueous solution as reference electrode fitted in a 0.2 cm pathlength quartz cuvette, as previously described and illustrated [26]. All potentials are expressed as versus Ag/AgCl. Both ellipticity and absorbance were monitored simultaneously and recorded between 195 and 225 nm with a spectral width of 1 nm. Measurements were performed with 0.8 ml sample volumes at the potentials indicated for 25 min and then followed with bias off for 10 min.

4.6. Use of perchloric acid

Perchloric acid was used to maintain reflectin in the monomeric state at the start of each experiment. Acidic pH previously had been shown necessary to maintain the protein's excess of cationic amino acid residues (His, Lys and Arg) in their fully charged state, thus ensuring the high Coulombic repulsion needed initially to prevent condensation, folding and assembly [16,23]. The choice of perchloric acid was dictated by its transparency in the far UV, in contrast with the high absorption of many other common acids, thus permitting sensitive, interference-free analyses of voltage-induced folding by CD.

Data accessibility. The data are provided in the electronic supplementary material [41].

Authors' contributions. Y.-C.L.: conceptualization, data curation, formal analysis, investigation, methodology and writing—original draft; E.M.: formal analysis, investigation, methodology and writing—review and editing; Y.A.S.: resources; L.S.: investigation, supervision and writing—review and editing; M.J.G.: investigation, supervision and writing—review and editing; D.E.M.: investigation, resources, supervision and writing—review and editing.

All authors gave final approval for publication and agreed to be held accountable for the work performed therein.

Conflict of interest declaration. The authors declare no competing interests.

Funding. Research was sponsored by the U.S. Army Research Office, grant nos. W911NF-20-1-0257 and W911NF-21-2-0068. The content of the information herein does not necessarily reflect the position or the policy of the US Government, and no official endorsement should be inferred.

References

1. Tao AR, DeMartini DG, Izumi M, Sweeney AM, Holt AL, Morse DE. 2010 The role of protein assembly in dynamically tunable bio-optical tissues. *Biomaterials* **31**, 793–801. (doi:10.1016/j.biomaterials.2009.10.038)
2. Hanlon R. 2007 Cephalopod dynamic camouflage. *Curr. Biol.* **17**, R400–R404. (doi:10.1016/j.cub.2007.03.034)
3. Hanlon RT, Chiao CC, Mäthger LM, Barbosa A, Buresch KC, Chubb C. 2009 Cephalopod dynamic camouflage: bridging the continuum between background matching and disruptive coloration. *Phil. Trans. R. Soc. B* **364**, 429–437. (doi:10.1098/rstb.2008.0270)
4. Mäthger LM, Bell GRR, Kuzirian AM, Allen JJ, Hanlon RT. 2012 How does the blue-ringed octopus (*Hapalochlaena lunulata*) flash its blue rings? *J. Exp. Biol.* **215**, 3752–3757. (doi:10.1242/jeb.076869)
5. Qin G *et al.* 2013 Recombinant reflectin-based optical materials. *J. Polym. Sci. B* **51**, 254–264. (doi:10.1002/polb.23204)
6. Phan L, Walkup iv WG, Ordinario DD, Karshalev E, Jocson JM, Burke AM, Gorodetsky AA. 2013 Reconfigurable infrared camouflage coatings from a cephalopod protein. *Adv. Mater.* **25**, 5621–5625. (doi:10.1002/adma.201301472)
7. Kreit E, Mäthger LM, Hanlon RT, Dennis PB, Naik RR, Forsythe E, Heikenfeld J. 2013 Biological versus electronic adaptive coloration: how can one inform the other? *J. R. Soc. Interface* **10**, 20120601. (doi:10.1098/rsif.2012.0601)
8. Yu C *et al.* 2014 Adaptive optoelectronic camouflage systems with designs inspired by cephalopod skins. *Proc. Natl Acad. Sci. USA* **111**, 12 998–13 003. (doi:10.1073/pnas.1410494111)
9. Crookes WJ, Ding LL, Huang QL, Kimbell JR, Horwitz J, McFall-Ngai MJ. 2004 Reflectins: the unusual proteins of squid reflective tissues. *Science* **303**, 235–238. (doi:10.1126/science.1091288)
10. Kramer RM, Crookes-Goodson WJ, Naik RR. 2007 The self-organizing properties of squid reflectin protein. *Nat. Mater.* **6**, 533–538. (doi:10.1038/nmat1930)
11. Izumi M *et al.* 2010 Changes in reflectin protein phosphorylation are associated with dynamic iridescence in squid. *J. R. Soc. Interface* **7**, 549–560. (doi:10.1098/rsif.2009.0299)
12. DeMartini DG, Krogstad DV, Morse DE. 2013 Membrane invaginations facilitate reversible water flux driving tunable iridescence in a dynamic biophotonic system. *Proc. Natl Acad. Sci. USA* **110**, 2552–2556. (doi:10.1073/pnas.1217260110)
13. DeMartini DG, Izumi M, Weaver AT, Pandolfi E, Morse DE. 2015 Structures, organization, and function of reflectin proteins in dynamically tunable reflective cells. *J. Biol. Chem.* **290**, 15 238–15 249. (doi:10.1074/jbc.M115.638254)
14. Ordinario DD *et al.* 2017 Protochromic devices from a cephalopod structural protein. *Adv. Opt. Mater.* **5**, 1600751. (doi:10.1002/adom.201600751)

15. Mäthger LM, Denton EJ, Marshall NJ, Hanlon RT. 2009 Mechanisms and behavioural functions of structural coloration in cephalopods. *J. R. Soc. Interface* **6**, S149–S163. (doi:10.1098/rsif.2008.0366.focus)
16. Levenson R, DeMartini DG, Morse DE. 2017 Molecular mechanism of reflectin's tunable biophotonic control: opportunities and limitations for new optoelectronics. *APL Mater.* **5**, 104801. (doi:10.1063/1.4985758)
17. Liang SP, Levenson R, Malady B, Gordon MJ, Morse DE, Sepunaru L. 2020 Electrochemistry as a surrogate for protein phosphorylation: voltage-controlled assembly of reflectin A1. *J. R. Soc. Interface* **17**, 20200774. (doi:10.1098/rsif.2020.0774)
18. Cooper KM, Hanlon RT, Budelmann BU. 1990 Physiological color change in squid iridophores. *Cell Tissue Res.* **259**, 15–24. (doi:10.1007/BF00571425)
19. Levenson R, Bracken C, Bush N, Morse DE. 2016 Cyclable condensation and hierarchical assembly of metastable reflectin proteins, the drivers of tunable biophotonics. *J. Biol. Chem.* **291**, 4058–4068. (doi:10.1074/jbc.M115.686014)
20. Hoffmann EK, Lambert IH, Pedersen SF. 2009 Physiology of cell volume regulation in vertebrates. *Physiol. Rev.* **89**, 193–277. (doi:10.1152/physrev.00037.2007)
21. Ghoshal A, DeMartini DG, Eck E, Morse DE. 2014 Experimental determination of refractive index of condensed reflectin in squid iridocytes. *J. R. Soc. Interface* **11**, 20140106. (doi:10.1098/rsif.2014.0106)
22. Xu C, Stiubianu GT, Gorodetsky AA. 2018 Adaptive infrared-reflecting systems inspired by cephalopods. *Science* **359**, 1495–1500. (doi:10.1126/science.aar5191)
23. Levenson R, Bracken C, Sharma C, Santos J, Arata C, Malady B, Morse DE. 2019 Calibration between trigger and color: neutralization of a genetically encoded coulombic switch and dynamic arrest precisely tune reflectin assembly. *J. Biol. Chem.* **294**, 16 804–16 815. (doi:10.1074/jbc.RA119.010339)
24. Naughton KL *et al.* 2016 Self-assembly of the cephalopod protein reflectin. *Adv. Mater.* **28**, 8405–8412. (doi:10.1002/adma.201601666)
25. Liang SP, Masquelier E, Morse DE, Gordon MJ, Sepunaru L. 2022 Low voltage voltammetry probes proton dissociation equilibria of amino acids and peptides. *Anal. Chem.* **94**, 4948–4953. (doi:10.1021/acs.analchem.1c03371)
26. Masquelier E, Liang S-P, Sepunaru L, Morse DE, Gordon MJ. 2022 Reversible electrochemical triggering and optical interrogation of polylysine α-helix formation. *Bioelectrochemistry* **144**, 108007. (doi:10.1016/j.bioelechem.2021.108007)
27. Costentin C, Canales JC, Haddou B, Savéant JM. 2013 Electrochemistry of acids on platinum: application to the reduction of carbon dioxide in the presence of pyridinium ion in water. *J. Am. Chem. Soc.* **135**, 17 671–17 674. (doi:10.1021/ja407988w)
28. Greenfield NJ, Fasman GD. 1969 Computed circular dichroism spectra for the evaluation of protein conformation. *Biochemistry* **8**, 4108–4116. (doi:10.1021/bi00838a031)
29. Rosenheck K, Doty P. 1961 The far ultraviolet absorption spectra of polypeptide and protein solutions and their dependence on conformation. *Proc. Natl Acad. Sci. USA* **47**, 1775–1785. (doi:10.1073/pnas.47.11.1775)
30. Moffitt W, Yang JT. 1956 The optical rotatory dispersion of simple polypeptides. I. *Proc. Natl Acad. Sci. USA* **42**, 596–603. (doi:10.1073/pnas.42.9.596)
31. Bayley PM. 1973 The analysis of circular dichroism of biomolecules. *Prog. Biophys. Mol. Biol.* **27**, 1–76. (doi:10.1016/0079-6107(73)90003-5)
32. Park C, Goddard WA. 2000 Stabilization of α-helices by dipole—dipole interactions within α-helices. *J. Phys. Chem. B* **104**, 7784–7789. (doi:10.1021/jp0001743)
33. Masquelier E, Taxon E, Liang SP, Al Sabeh Y, Sepunaru L, Gordon MJ, Morse DE. 2023 A new electrochemical method that mimics phosphorylation of the core tau peptide K18 enables kinetic and structural analysis of intermediates and assembly. *J. Biol. Chem.* **299**, 103011. (doi:10.1016/j.jbc.2023.103011)
34. Wong IY, Footer MJ, Melosh NA. 2008 Electronically activated actin protein polymerization and alignment. *J. Am. Chem. Soc.* **130**, 7908–7915. (doi:10.1021/ja7103284)
35. Kang K, Platten F. 2022 Electric-field induced modulation of amorphous protein aggregates: polarization, deformation, and reorientation. *Sci. Rep.* **12**, 3061. (doi:10.1038/s41598-022-06995-x)
36. Wang M, Falke S, Schubert R, Lorenzen K, Cheng Q-d, Exner C, Brognaro H, Mudogo CN, Betzel C. 2020 Pulsed electric fields induce modulation of protein liquid–liquid phase separation. *Soft Matter* **16**, 8547–8553. (doi:10.1039/D0SM01478H)
37. Yuan Z, Wu M, Meng Y, Niu Y, Xiao W, Ruan X, He G, Jiang X. 2022 Protein crystal regulation and harvest via electric field-based method. *Curr. Opin. Chem. Eng.* **36**, 100744. (doi:10.1016/j.coche.2021.100744)
38. Liu Y, Xi Y. 2019 Colloidal systems with a short-range attraction and long-range repulsion: phase diagrams, structures, and dynamics. *Curr. Opin. Colloid Interface Sci.* **39**, 123–136. (doi:10.1016/j.cocis.2019.01.016)
39. Levenson R, Malady B, Lee T, Sabeh YA, Kohl P, Li Y, Morse DE. 2021 Protein charge neutralization is the proximate driver dynamically tuning a nanoscale Bragg reflector. *bioRxiv*. (doi:10.1101/2021.04.23.441158)
40. Bard AJ, Faulkner LR. 2001 *Electrochemical methods: fundamentals and applications*, 2nd edn. New York, NY: Wiley.
41. Lin Y-C, Masquelier E, Sabeh YA, Sepunaru L, Gordon MJ, Morse DE. 2023 Voltage-calibrated, finely tunable protein assembly. Figshare. (doi:10.6084/m9.figshare.c.6707535)